Atomic Resolution of Calcium and Oxygen Sublattices of Calcite in Ambient Conditions by Atomic Force Microscopy Using qPlus Sensors with Sapphire Tips

Daniel S. Wastl,* Michael Judmann, Alfred J. Weymouth, and Franz J. Giessibl

Institute of Experimental and Applied Physics, University of Regensburg, Universitätsstrasse 31, 93053 Regensburg, Germany

ABSTRACT Characterization and imaging at the atomic scale with atomic force microscopy in biocompatible environments is an ongoing challenge. We demonstrate atomically resolved imaging of the calcite ($10\bar{1}4$) surface plane using stiff quartz cantilevers ("qPlus sensors", stiffness $k = 1280$ N/m) equipped with sapphire tips in ambient conditions without any surface preparation. With 10 atoms in one surface unit cell, calcite has a highly complex surface structure comprising three different chemical elements (Ca, C, and O). We obtain true atomic resolution of calcite in air at relative humidity ranging from 20% to 40%, imaging atomic steps and single atomic defects. We observe a great durability of sapphire tips with their Mohs hardness of 9, only one step below diamond. Depending on the state of the sapphire tip, we resolve either the calcium or the oxygen sublattice. We determine the tip termination by comparing the experimental images with simulations and discuss the possibility of chemical tip identification in air. The main challenges for imaging arise from the presence of water layers, which form on almost all surfaces and have the potential to dissolve the crystal surface. Frequency shift *versus* distance spectra show the presence of at least three ordered hydration layers. The measured height of the first hydration layer corresponds well to X-ray diffraction data and molecular dynamic simulations, namely, ~220 pm. For the following hydration layers we measure ~380 pm for the second and third layer, ending up in a total hydration layer thickness of at least 1 nm. Understanding the influence of water layers and their structure is important for surface segregation, surface reactions including reconstructions, healing of defects, and corrosion.

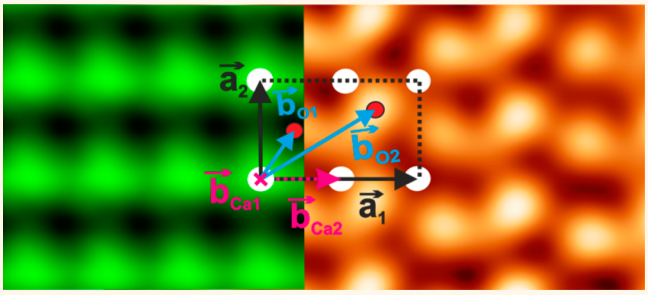

KEYWORDS: atomic resolution · qPlus · calcite · atomic force microscopy (AFM) · ambient conditions

The increasing interest in nanostructures, nanoparticles, and the structure and properties of biological and chemical samples in natural environments creates a need for imaging tools that are capable of resolving at the atomic and intermolecular scales in ambient conditions.[1−6]

In ambient conditions, surfaces are exposed directly to laboratory air with all its pollutants and gas components. Ambient air contains a significant amount of water vapor, where the partial pressure of water depends on temperature and relative humidity (RH). If humidity is present, all surfaces (hydrophobic or hydrophilic) exposed to air adsorb a water layer.[7−10] The water layer can cause both dissolution and recrystallization of the surface.[11−16] The thickness of the water condensation layer is dependent on the exposure time, temperature, RH, and the sample's hydrophilic or hydrophobic character.[6,9,10,17−20] Depending on the sample, ordered hydration layers can be present. On ionic crystals, the water molecules often form ordered water layers with a characteristic structure on the sample surface.[10,21,22] The thickness of single ordered hydration layers on various samples is reported to range from 200 to 345 pm.

One method to achieve high resolution in these environments is atomic force

* Address correspondence to daniel.wastl@physik.uni-regensburg.de.

Received for review December 2, 2014 and accepted March 27, 2015.

Published online March 27, 2015
10.1021/acsnano.5b01549

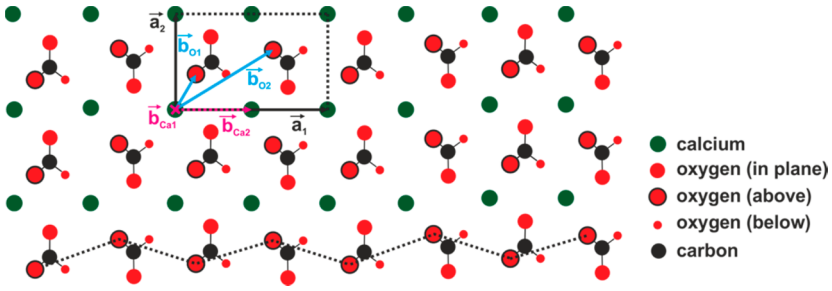

Figure 1. Calcite ($CaCO_3$) ($10\bar{1}4$) cleavage plane. (a) Schematic drawing of the ($10\bar{1}4$) cleavage plane. The surface unit cell is indicated by the unit vectors (a_1, a_2) pointing to the calcium ions (Ca^{2+}) and the basis vectors (b_{Ca1}, b_{Ca2}, b_{O1}, b_{O2}). b_{Ca1} is the zero vector; b_{Ca2} a vector with half the length of a_1 pointing to calcium ions. The vectors b_{O1} and b_{O2} mark the position of the protruding oxygen atoms. The dashed line shows the zigzag structure of the protruding oxygen atoms.

microscopy (AFM).[23−25] The highest spatial resolution is realized in ultrahigh vacuum (UHV) with the atomic force microscope, where the environment is highly controlled and stable operation over days is possible. Imaging down to the atomic scale is also possible in liquid[1,26,27] and ambient conditions,[6,10] but the vaguely defined surface contamination films that are present in these environments are a challenge. One possibility to work in biocompatible conditions is to immerse the whole system, *i.e.*, sensor and sample, in a buffer solution. In this case, the quality factor (Q) of completely immersed sensors decreases dramatically down to single-digit values, which has a large effect on the overall noise in the measurements.[28,29] In our approach, we use relatively large and stiff qPlus sensors in ambient conditions where only the tip penetrates the adsorption layer(s), thus reaching high signal-to-noise values with moderately high Q values even in the presence of ordered hydration layers and the liquid water condensate phase.[10] If a hydration layer or condensation layer is present, only the front-most part of the tip is immersed, which leads to Q values of 100−800 during sample contact. The actual Q value depends on the condensation layer height and structure, the tip's sharpness, and the sample system.[6,10]

Here we use calcite as a test system for high resolution in biorelevant environments. Calcite is the most stable polymorph of $CaCO_3$. It is abundant in geological environments and is an important mineral in a wide range of fields. It plays a crucial role in biomineralization, where crystal growth is controlled by the presence of biological macromolecules.[30,31] $CaCO_3$ is used in a number of industrial products, namely, paint, cement, cosmetics, paper, pharmaceuticals, and, due to its birefringence, optical devices.[27] Moreover, calcite has been discussed in the context of homochirality of life, as enantiospecific adsorption of natural amino acids to calcite surfaces has been demonstrated.[32−34]

Calcite has a rhombohedrical crystal structure. The most stable cleavage plane is the ($10\bar{1}4$) plane. Calcite is a layered material[35] with strong bonds holding the ions together within one layer and weak bonding between layers. The ($10\bar{1}4$) surface is a natural cleavage plane because of its weak bonds perpendicular to this plane and the closely packed arrangement of calcium and carbonate ions along the layer.[36] A crack can propagate along a minimum-energy pathway with minimum dispersion of energy.[37]

The surface unit cell of the calcite ($10\bar{1}4$) cleavage plane is shown in Figure 1 by the vectors a_1 and a_2 ($|a_1| = 0.81$ nm and $|a_2| = 0.5$ nm).[27,36] It consists of two calcium ions (Ca^{2+}) (dark green in Figure 1) and two carbonate groups (CO_3^{2-}). The carbonate groups are planar with one oxygen atom within the ($10\bar{1}4$) cleavage plane, one atom 80 pm below the plane, and one atom 80 pm above the plane.[38] This is indicated in Figure 1 by the size difference of the red circles. The dashed line in Figure 1a shows the zigzag structure of the protruding oxygen atoms along the horizontal direction.

The surface unit cell consists of two $CaCO_3$ units, *i.e.*, 10 atoms. Out of these 10, only four atoms are at the surface and thus relevant for the AFM contrast. For clarity we depict only these four relevant basis vectors in Figure 1. The basis vectors b_{Ca1}, b_{Ca2}, b_{O1}, and b_{O2} describe the relative position of the aforementioned four atoms. With our choice of the lattice originating in the first calcium atom, b_{Ca1} and b_{Ca2} mark the positions of the calcium ions and b_{O1} and b_{O2} mark the position of the protruding oxygen atoms.

The surface structure of the calcite ($10\bar{1}4$) cleavage plane has been studied in ultrahigh vacuum, ambient, and liquid conditions with various techniques.[36,39−43] Using contact mode AFM, the rectangular lattice of the calcium ions[36] and the characteristic zigzag structure of the protruding oxygen atoms[41] were observed. These are the two most common structures observed in AFM experiments on calcite.[27,36,40] While the calcite sublattices have been reported, the imaging mechanism was not clarified.

In this work, we show true atomic resolution of the calcite ($10\bar{1}4$) cleavage plane with very stiff cantilevers (1280 N/m, qPlus sensors[6,9,10,44,45]) equipped with sapphire tips directly in air without using a buffer solution. We show atomic defects of the so-called

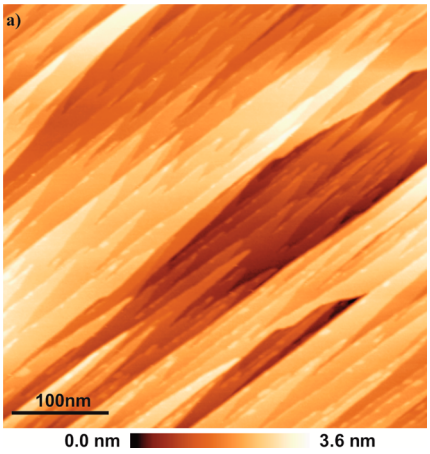

Figure 2. Calcite ($CaCO_3$) ($10\bar{1}4$) cleavage plane. Overview image of freshly cleaved calcite ($CaCO_3$) ($10\bar{1}4$) in air. Single and multiple atomic steps are visible with a step height of ~300 pm (literature value 316 pm[36]). The crystal is cleaved with a razor blade, known to produce an atomically smooth surface. Scan parameters: sapphire tip, k = 1280 N/m, Δf = +9 Hz, A = 500 pm.

zigzag structure where a single oxygen atom is missing, and we show atomic steps with atomic resolution. Frequency *versus* distance spectra show the existence of at least three ordered hydration layers on top of the $CaCO_3$ ($10\bar{1}4$) cleavage plane. The thickness of the hydration layers is comparable with previous published molecular dynamic (MD) simulations and X-ray scattering experiments. We confirm the two reported imaging contrasts on the ($10\bar{1}4$) cleavage plane, *i.e.*, zigzag structure corresponding to the oxygen sublattice and a rectangular structure corresponding to the calcium sublattice. By simulating the imaging process, we can show that the imaging contrast depends on the tip state.

RESULTS AND DISCUSSION

Our samples are prepared by cleaving the calcite crystal before each scan session. Figure 2 shows an overview image of such a cleaved calcite ($10\bar{1}4$) surface in air. We observe a clean surface with steps with a step height of ~316 pm corresponding to single atomic steps. The sensor was equipped with a sapphire tip.[6,10] Etched tungsten (Mohs hardness 7.5) and silicon (Mohs hardnes 7) have been tested before, but failed to achieve atomic resolution on calcite. We found silicon and tungsten to be not robust enough for scanning calcite in air. Sapphire (Al_2O_3), with a Mohs hardness of 9, two steps harder than commonly used silicon and only one step below diamond (Mohs hardness 10), is very robust on various surfaces and has been successfully used before for imaging graphene[6] and ionic crystals[10] with atomic resolution. We have also fabricated and tested diamond tips on qPlus sensors, but we have not obtained good atomic resolution so far. We speculate that diamond tips ending in a single atom might locally rehybridize to form

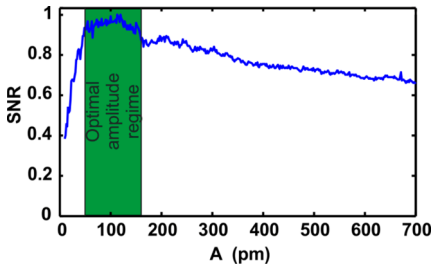

Figure 3. Normalized signal-to-noise spectrum of the sapphire tip on the calcite ($10\bar{1}4$) cleavage plane. The optimal amplitude regime is marked in green. Within this regime the best atomic resolution images are obtained. The spectrum was calculated with the method described by Wastl *et al.*[10]

graphite under the high local pressure at the tip apex. Graphite is known to have a slightly larger bonding energy per atom than diamond. As far as we know, sapphire does not reconstruct into an energetically more favorable structure under high loads. Aside from its hardness, sapphire is a unique tip material, as it is chemically inert under usual AFM conditions ($T \approx 4-300$ K), as well as resistant against etching with common acids.[46] Therefore, it is the tip of choice for all scanning environments including extreme conditions.

Recently we introduced a technique called *Q*-spectroscopy[10] that optimizes the scan parameters for high-resolution imaging directly in air. This technique builds on the discovery that the optimal oscillation amplitude is approximately equal to the decay length of the interaction that is probed,[47] modified by a strong influence of Q variations with amplitude. These variations of the Q value are caused by the liquid water phase and the hydration layer structure on the surface. In Figure 3 we show the normalized signal-to-noise ratio (SNR) as a function of amplitude for the sapphire tip used for atomic resolution. The SNR shows a plateau for amplitudes of 50 pm < A_{opt} < 160 pm, indicating the optimal amplitude regime for atomic resolution.[6,10] At these small amplitudes the tip oscillates within a single hydration layer.

Figure 4 shows a frequency shift (Δf) *versus* distance (z) spectrum measured while obtaining atomic resolution. The start of the interaction between the sapphire tip and the water condensation layer on the calcite surface is at a distance of 14 nm. The initially attractive interaction (negative frequency shift) prevails, which is most likely due to meniscus forces, van der Waals interaction, or long-range electrostatic interaction.[10] Closer to the surface, the spectrum clearly shows three undulations, with peaks labeled H1, H2 and H3. These peaks correspond to ordered water molecules, which apparently form the ("ice-like") hydration layers[48] on the calcite ($10\bar{1}4$) cleavage plane. The corresponding force is known as the structural hydration force.[49,50] We measured hydration layer thicknesses of d_{H1} = 220 pm for the first hydration layer and $d_{H2,H3}$ = 380 pm for the second layer and third layer. Previous molecular

dynamics simulations including bulk water layers with nanometer thickness suggest the presence of at least two ordered hydration layers on the calcite ($10\bar{1}4$) cleavage plane.[51−53] Recently Imada *et al.* reported three ion-specific ordered hydration layers, measured by FM-AFM, on the ($10\bar{1}4$) cleavage plane in buffer solution.[54] The value d_{H1} = 220 pm we measured for the first hydration layer fits well with values of the molecular dynamics simulations[51−53] and the ∼220−250 pm Fenter[42,55] *et al.* and Geissbühler[43] *et al.* found with X-ray scattering.

The thickness difference of the hydration layers (from the first to the following hydration layers) on calcite can be the result of various effects. First, the influence of the ionic surface decays with increasing distance. With increasing distance, the hydration layers are less ordered. Second, the ion concentration in the hydration layers could vary, which might lead to a thickness variation due to ion hydration.[56] This ion-dependent hydration effect and the relation to the hydration layer thickness were recently shown by Δf *versus* z spectra on a mica−electrolyte interface.[56] Summing up the individual ordered hydration layer heights on calcite results in a total thickness of almost 1 nm.

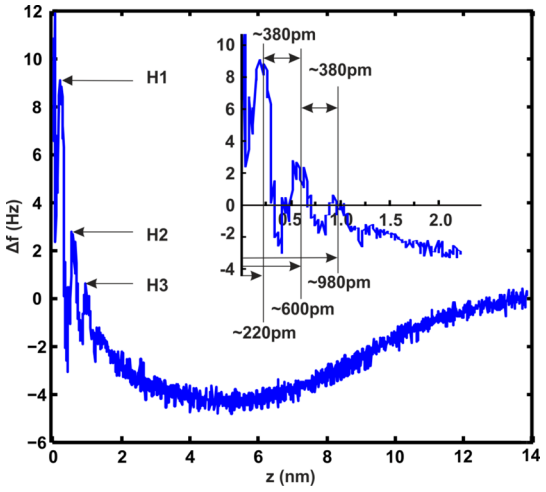

Figure 4. Frequency shift (Δf) *versus* distance (z) spectrum. In the spectrum we observe at least three undulations, with peaks indicated by H1, H2, and H3. The peaks correspond to the first three hydration layers on the calcite ($10\bar{1}4$) cleavage plane. The thicknesses are H1 ≈ 220 pm and H2 and H3 ≈ 380 pm. The height variation can be related to the presence of dissolved ions in the ordered hydration layers.

Figure 5 shows line-flattened topographic raw data of the rectangular and zigzag surface lattices on the calcite ($10\bar{1}4$) cleavage plane. In Figure 5a the protruding oxygen atoms are imaged where the protrusions are aligned to make zigzag lines along the [$\bar{4}\bar{2}1$] direction. This feature has been reported before, and the zigzag truncated bulk structure of the oxygen atoms is also known as row pairing.[27,36,40,41,54]

Figure 5b shows the rectangular structure with half the lattice spacing in the [$\bar{4}\bar{2}1$] direction. This contrast can be understood by ascribing the imaged features to the calcium ions instead of the protruding oxygen atoms.[11,27]

In Figure 6, we demonstrate true atomic resolution by imaging a single atomic defect and a single atomic step with atomic resolution on both terraces. In Figure 6a, the missing atom in the zigzag structure is clearly observable. This atomic defect is marked by a white arrow and shows true atomic resolution while scanning with a stable sapphire tip. Figure 6b shows an atomically resolved step. The atoms can be imaged on both terraces. The step height, which can be seen in the line scan in Figure 6c, corresponds well with the literature value of 316 pm. The fringes at the atomically resolved step edge result from the long-range contributions, namely, van der Waals force or electrostatic forces, and have been reported earlier in UHV observations.[57]

To clarify the imaging mechanism on calcite in air, we simulated the interactions between the tip and surface while oscillating in close proximity to the

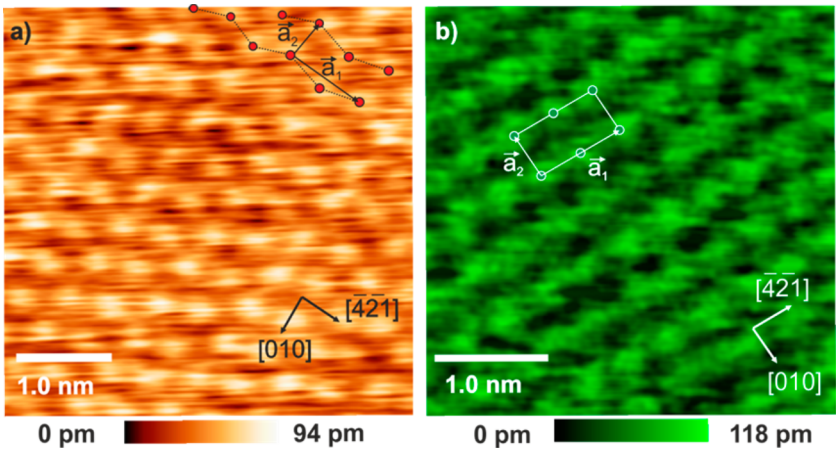

Figure 5. Observable atomic structures on the calcite ($10\bar{1}4$) cleavage plane in air. (a) Zigzag structure of the protuding oxygen atoms (see Figure 1 for unit cell). Scan parameters: Δf = 138 Hz, A = 118 pm. (b) Calcium sublattice.[68] Scan parameters: Δf = 100 Hz, A = 118 pm.

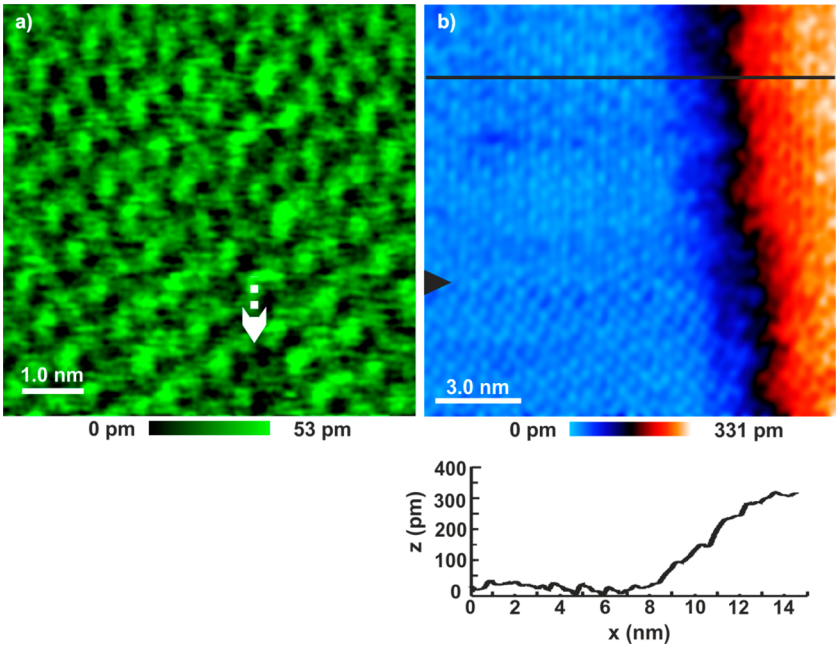

Figure 6. True atomic resolution of the calcite (10$\bar{1}$4) cleavage plane in air. (a) Zigzag structure of the protruding oxygen atoms' with single atomic defect marked by an arrow. There is an oxygen atom missing. Scan parameters: Δf = 100 Hz, A = 150 pm. (b) Atomic step with atomic resolution on both terraces of calcite in air. The atomic resolution of the step edge represents true atomic resolution imaging. A tip change is marked with a black arrow. Scan parameters: Δf = 260 Hz, A = 117 pm.

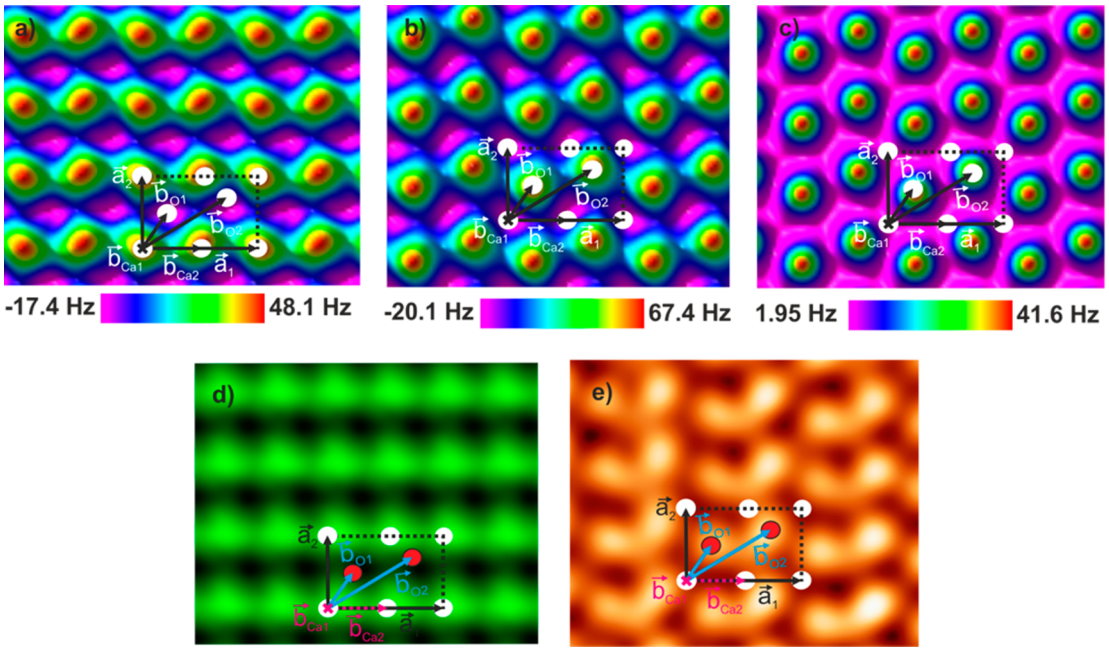

Figure 7. Various observable structures of the calcite (10$\bar{1}$4) surface: Data and simulations. (a, b and c) Simulation of the frequency shift due to Pauli repulsion and the electrostatic force between the calcite (10$\bar{1}$4) surface and (a) double positively charged tip (Ca^{2+}) and (b) negatively charged tip (CO_3^{2-}) simulating an oxygen atom as the front atom. (c) Simulation of the frequency shift due to Pauli repulsion (uncharged tip). The simulated tip−sample distance is 350 pm. (d) Filtered, lattice-averaged real data of the rectangular lattice of the calcium ions (Ca^{2+}). (e) Filtered lattice-averaged real data of the lattice of the protruding oxygen atoms.

surface. The goal of this is to understand the atomic-scale contrast, not to reproduce the entire tip−sample interaction. From our investigation of the hydration layers, discussed in reference to Figure 4, we know that when scanning with Δf > 20 Hz the tip has penetrated the hydration layers and that no water layer exists between the apex and the surface. This is the case for the images shown in Figures 5 to 7. As described in the work of Watkins and Shluger,[58] there are three major interactions that need to be considered when

simulating AFM images in water: direct tip−sample interaction, similar to that in UHV; the cost to displace water on the surface from preferred surface locations; and interaction when water is trapped between the tip and the sample. As we have penetrated the hydration layers, there are no trapped molecules directly under the tip apex. Furthermore, the lateral scan motion of the tip is much slower than the vertical oscillation, and we will not consider the net lateral displacement of water molecules when acquiring an AFM image. We therefore concentrate on the direct tip−sample interaction, in which it is known (from UHV experiments) that the front atom or ion of the tip determines the imaging contrast.[57,59,60]

On ionic crystals, surface material can be easily picked up or dropped.[27,60] The tip apex is most likely contaminated by surface material while scanning. The tip termination can change during scanning or be changed on purpose with slight pokes of the tip to the sample surface.[6,10] Therefore, on calcite it is highly likely that the tip is either charged positively (Al^{3+}, Ca^{2+}) or negatively (O^{2-}, CO_3^{2-}) charged or saturated with adsorbates and possibly more or less neutral.

We simulated the three most probable different tip terminations: Ca^{2+}, O^{-}, and neutral. We model the electrostatic interaction and the Pauli repulsion. The charge density of calcite that we used for the simulation of the electrostatic interaction was calculated by Pavese *et al.*[61] The tip was modeled by a point charge that interacted with all surface atoms. The electrostatic forces (F_{el}) were described with the Coulomb interaction $F_C = q_1 q_2 / (4\pi\varepsilon_0 r^2)$. In order to incorporate the effect of the water upon the electrostatic interactions, we included a weighting function based upon the Debye screening length, λ_D: $\exp(-r/\lambda_D)$. Calcite is not highly dissolvable in water at ambient conditions,[62] and ionic concentrations around 0.001 mol/L are expected. A concentration of 0.001 mol/L results in a Debye length of $\lambda_D = 9.6$ nm. We also simulated higher ionic concentrations and found no significant change in the output as the Debye length depends only on the square root of the inverse concentration. Furthermore, this weighting function does not significantly change the interaction between the apex atom of the tip and the nearest surface atoms, but rather screens the effect of further surface atoms. For the calculation of the interaction due to the Pauli repulsion we used the potential

$$V_P = V_0 \exp(-(r - r_0)/\lambda) \quad (1)$$

with $V_0 = 0.77$ eV, $\lambda = 25$ pm, and $r_0 = 240$ pm.[38,61,63,64]

The frequency shift (Δf) is calculated by $\Delta f(z,A) = [f_0/(kA^{3/2}]\gamma(z,A)$, where f_0 and k are the eigenfrequency and the stiffness of the sensor, A is the oscillation amplitude, and $\gamma(z,A)$ is the normalized frequency shift.[65] Although the amplitudes used in this study are small compared to amplitudes used with traditional silicon cantilevers, compared to the decay contrast of the Pauli repulsion (~25 pm), they are relatively large. To calculate $\gamma(z,A)$ resulting from the Pauli repulsion, we used the large-amplitude approximation $\gamma_{la}(z) = F_{Pauli}(z)(\lambda/2\pi)^{1/2}$, which is valid for the amplitudes used in our measurements and has been described previously.[66] The normalized frequency shift $\gamma(z,A)$ for a tip interacting *via* the electrostatic force while directly above a charged adsorbate is given by[66]

$$\gamma(z,A) = F_{el}(z)A^{0.5}\{F[2, 0.5, 1](-2A/z) - F[2, 1.5, 2](-2A/z)\} \quad (2)$$

$F[a,b,c]$ is the hypergeometric function.[67] To adapt it to our three-dimensional model, we allowed F_{el} to be a function of x, y, and z. We fixed the z value in the hypergeometric functions at $z_0 = 350$ pm, which fits best with the obtained contrast of our atomically resolved images.

Figure 7a−c shows the results of the simulation. The basis vectors are shown for clarity in each image. The simulation shows, depending on the charge state of the tip's front atom, one can image either the rectangular lattice of the calcium ions (positively charged tip, see Figure 7a) or the zigzag structure of the protruding oxygen atoms (negatively or neutral charged tip, see Figure 7b and c). The results of the simulation shown in Figure 7a−c fit well with the measured topographic AFM data shown in Figure 7d and e. The topographic data in Figure 7d and c are filtered, lattice-averaged experimental data of the calcite surface for two different tip terminations. As shown by the simulations, the kind of ions that are imaged as protrusions form a rectangular lattice of calcium ions (Ca^{2+}) if the tip is positively charged (Figure 7d) or the lattice of the protruding oxygen atoms of the CO_3^{2-} ions for a negatively or neutral charged tip (Figure 7e). From comparison of the simulations and AFM data of the calcium sublattice, we clearly can identify a positively charged (Al^{3+}, Ca^{2+}) tip. This opens the possibility of chemical tip identification in air.

CONCLUSION

We discovered the presence of three ice-like water layers on the calcite ($10\bar{1}4$) cleavage plane at room temperature under normal laboratory conditions using frequency *versus* distance spectra. While oscillating with small optimized amplitudes in the first hydration layers, we are able to scan with true atomic resolution directly in air without any special treatment of the sample. We have confirmed the presence of two distinct appearances of the calcite surface that had been reported in the literature before, and we imaged a single atomic step with atomic resolution and an atomic defect in the zigzag structure. We can show the existence of ordered hydration layers with high precision to their thickness. This opens a wide field of additional experiments, related to hydration effects

on surfaces and nanoparticles as well as biological and chemical sample structures. As calcite is used for biological applications, this work is a demonstration of high resolution in biological environments. The hardness of sapphire is not the only advantage of the new kind of tip material. It is chemically inert and acid resistant. The possibility of true atomic resolution with chemically identified tips in air opens a variety of new experiments with high resolution in realistic environments.

MATERIALS AND METHODS

Quartz Cantilever AFM. The AFM experiments were performed on a laboratory-built qPlus ambient AFM,[9,10] operated by a Nanonis Control System with an OC4 PLL from SPECS GmbH. We used custom-designed qPlus sensors that are manufactured similar to quartz tuning-forks. The used sensors have a characteristic bare resonance frequency of f_0 = 32 768 Hz and a stiffness k = 1280 N/m.[6,10] The qPlus sensors were equipped with sapphire tips, made by splintering bulk crystals. Sensor parameters: f_0 = 32169 Hz, Q_{air} = 1760 bulk sapphire tip. The amplitudes are optimized by Q-spectroscopy.

***Q*-Spectroscopy.** The imaging amplitude A was optimized by a method described in detail in a previous publication.[10] Drive amplitude *versus* amplitude spectra are taken close to the sample and far away in air. Using these spectra, one can calculate the energy loss per oscillation cycle and the effective Q value for the actual tip sample configuration.

Conflict of Interest: The authors declare no competing financial interest.

Acknowledgment. Financial support from the Deutsche Forschungsgemeinschaft (GRK 1570) is gratefully acknowledged. F.J.G. and D.S.W. conceived of the experiments. M.J. and D.S.W. performed the experiments. F.J.G., D.S.W., M.J., and A.J.W. were involved in simulation, interpretation, discussion, and paper writing.

REFERENCES AND NOTES

1. Fukuma, T.; Kobayashi, K.; Matsushige, K.; Yamada, H. True Atomic Resolution in Liquid by Frequency-Modulation Atomic Force Microscopy. *Appl. Phys. Lett.* **2005**, *87*, 034101.
2. Schreiber, M.; Eckardt, M.; Klassen, S.; Adam, H.; Nalbach, M.; Greifenstein, L.; Kling, F.; Kittelmann, M.; Bechstein, R.; Kühnle, A. How Deprotonation Changes Molecular Self-Assembly – an AFM Study in Liquid Environment. *Soft Matter* **2013**, *9*, 7145.
3. Yoo, P. J.; Nam, K. T.; Qi, J.; Lee, S.-K.; Park, J.; Belcher, A. M.; Hammond, P. T. Spontaneous Assembly of Viruses on Multilayered Polymer Surfaces. *Nat. Mater.* **2006**, *5*, 234–240.
4. Hahnel, S.; Wastl, D. S.; Schneider-Feyrer, S.; Giessibl, F. J.; Brambilla, E.; Cazzaniga, G.; Ionescu, A. Streptococcus Mutans Biofilm Formation and Release of Fluoride from Experimental Resin-Based Composites Depending on Surface Treatment and S-PRG Filler Particle Fraction. *J. Adhes. Dent.* **2014**, *16*, 313–321.
5. Ionescu, A.; Brambilla, E.; Wastl, D. S.; Giessibl, F. J.; Cazzaniga, G.; Schneider-Feyrer, S.; Hahnel, S. Influence of Matrix and Filler Fraction on Biofilm Formation on the Surface of Experimental Resin-Based Composites. *J. Mater. Sci. Mater. Med.* **2015**, *26*, 5372.
6. Wastl, D. S.; Weymouth, A. J.; Giessibl, F. J. Atomically Resolved Graphitic Surfaces in Air by Atomic Force Microscopy. *ACS Nano* **2014**, *8*, 5233–5239.
7. Palasantzas, G.; Svetovoy, V.; van Zwol, P. Influence of Ultrathin Water Layer on the van Der Waals/Casimir Force between Gold Surfaces. *Phys. Rev. B* **2009**, *79*, 235434.
8. James, M.; Darwish, T. a.; Ciampi, S.; Sylvester, S. O.; Zhang, Z.; Ng, A.; Gooding, J. J.; Hanley, T. L. Nanoscale Condensation of Water on Self-Assembled Monolayers. *Soft Matter* **2011**, *7*, 5309.
9. Wastl, D. S.; Speck, F.; Wutscher, E.; Ostler, M.; Seyller, T.; Giessibl, F. J. Observation of 4 nm Pitch Stripe Domains Formed by Exposing Graphene to Ambient Air. *ACS Nano* **2013**, *7*, 10032–10037.
10. Wastl, D. S.; Weymouth, A. J.; Giessibl, F. J. Optimizing Atomic Resolution of Force Microscopy in Ambient Conditions. *Phys. Rev. B* **2013**, *87*, 245415.
11. Hillner, P. E.; Manne, S.; Gratz, A. J.; Hansma, P. K. AFM Images of Dissolution and Growth on a Calcite Crystal. *Ultramicroscopy* **1992**, *42–44*, 1387–1393.
12. Baltrusaitis, J.; Grassian, V. H. Calcite Surface in Humid Environments. *Surf. Sci.* **2009**, *603*, L99–L104.
13. Perdikouri, C.; Putnis, C. V.; Kasioptas, A.; Putnis, A. An Atomic Force Microscopy Study of the Growth of a Calcite Surface as a Function of Calcium/Total Carbonate Concentration Ratio in Solution at Constant Supersaturation. *Cryst. Growth Des.* **2009**, *9*, 4344–4350.
14. Pina, C. M.; Merkel, C.; Jordan, G. On the Bimodal Effects of Silicic Acids on Calcite Growth. *Cryst. Growth Des.* **2009**, *9*, 4084–4090.
15. Ruiz-Agudo, E.; Putnis, C. V.; Jiménez-López, C.; Rodriguez-Navarro, C. An Atomic Force Microscopy Study of Calcite Dissolution in Saline Solutions: The Role of Magnesium Ions. *Geochim. Cosmochim. Acta* **2009**, *73*, 3201–3217.
16. Henriksen, K.; Stipp, S. L. S. Controlling Biomineralization: The Effect of Solution Composition on Coccolith Polysaccharide Functionality. *Cryst. Growth Des.* **2009**, *9*, 2088–2097.
17. Davy, S.; Spajer, M.; Courjon, D. Influence of the Water Layer on the Shear Force Damping in near-Field Microscopy. *Appl. Phys. Lett.* **1998**, *73*, 2594.
18. Wei, P. K.; Fann, W. S. The Effect of Humidity on Probe-Sample Interactions in near-Field Scanning Optical Microscopy. *J. Appl. Phys.* **2000**, *87*, 2561.
19. Huang, F. M.; Culfaz, F.; Festy, F.; Richards, D. Effect of the Surface Water Layer on the Optical Signal in Apertureless Scanning near Field Optical Microscopy. *Nanotechnology* **2007**, *18*, 015501.
20. Freund, J.; Halbritter, J.; Hörber, J. K. How Dry Are Dried Samples? Water Adsorption Measured by STM. *Microsc. Res. Technol.* **1999**, *44*, 327–338.
21. Kimura, K.; Ido, S.; Oyabu, N.; Kobayashi, K.; Hirata, Y.; Imai, T.; Yamada, H. Visualizing Water Molecule Distribution by Atomic Force Microscopy. *J. Chem. Phys.* **2010**, *132*, 194705.
22. Labuda, A.; Kobayashi, K.; Suzuki, K.; Yamada, H.; Grütter, P. Monotonic Damping in Nanoscopic Hydration Experiments. *Phys. Rev. Lett.* **2013**, *110*, 066102.
23. Gross, L.; Mohn, F.; Moll, N.; Meyer, G.; Ebel, R.; Abdel-Mageed, W. M.; Jaspars, M. Organic Structure Determination Using Atomic-Resolution Scanning Probe Microscopy. *Nat. Chem.* **2010**, *2*, 821–825.
24. Binnig, G.; Quate, C. F. Atomic Force Microscope. *Phys. Rev. Lett.* **1986**, *56*, 930–933.
25. Giessibl, F. J. Atomic Resolution of the Silicon (111)-(7×7) Surface by Atomic Force Microscopy. *Science* **1995**, *267*, 68–71.
26. Ichii, T.; Fujimura, M.; Negami, M.; Murase, K.; Sugimura, H. Frequency Modulation Atomic Force Microscopy in Ionic Liquid Using Quartz Tuning Fork Sensors. *Jpn. J. Appl. Phys.* **2012**, *51*, 08KB08.
27. Rode, S.; Oyabu, N.; Kobayashi, K.; Yamada, H.; Kühnle, A. True Atomic-Resolution Imaging of (1014) Calcite in Aqueous Solution by Frequency Modulation Atomic Force Microscopy. *Langmuir* **2009**, *25*, 2850–2853.

28. Albrecht, T. R.; Grütter, P.; Horne, D.; Rugar, D. Frequency Modulation Detection Using High-Q Cantilevers for Enhanced Force Microscope Sensitivity. *J. Appl. Phys.* **1991**, *69*, 668–673.
29. Kobayashi, K.; Yamada, H.; Matsushige, K. Frequency Noise in Frequency Modulation Atomic Force Microscopy. *Rev. Sci. Instrum.* **2009**, *80*, 043708.
30. Addadi, L.; Weiner, S. Control and Design Principles in Biological Mineralization. *Angew. Chem., Int. Ed. Engl.* **1992**, *31*, 153–169.
31. Cölfen, H. Precipitation of Carbonates: Recent Progress in Controlled Production of Complex Shapes. *Curr. Opin. Colloid Interface Sci.* **2003**, *8*, 23–31.
32. Addadi, L.; Weiner, S. Crystals, Asymmetry and Life. *Nature* **2001**, *411* (753), 755.
33. Hazen, R. M.; Filley, T. R.; Goodfriend, G. A. Selective Adsorption of L- and D-Amino Acids on Calcite: Implications for Biochemical Homochirality. *Proc. Natl. Acad. Sci. U.S.A.* **2001**, *98*, 5487–5490.
34. Orme, C. A.; Noy, A.; Wierzbicki, A.; McBride, M. T.; Grantham, M.; Teng, H. H.; Dove, P. M.; DeYoreo, J. J. Formation of Chiral Morphologies through Selective Binding of Amino Acids to Calcite Surface Steps. *Nature* **2001**, *411*, 775–779.
35. Hartman, P.; Perdok, W. G. On the Relations between Structure and Morphology of Crystals. I. *Acta Crystallogr.* **1955**, *8*, 49–52.
36. Ohnesorge, F.; Binnig, G. True Atomic Resolution by Atomic Force Microscopy through Repulsive and Attractive Forces. *Science* **1993**, *260*, 1451–1456.
37. Lawn, B. *Fracture of Brittle Solids*; Cambridge University Press: Cambridge, 1993.
38. Stipp, S. Toward a Conceptual Model of the Calcite Surface: Hydration, Hydrolysis, and Surface Potential. *Geochim. Cosmochim. Acta* **1999**, *63*, 3121–3131.
39. Stipp, S. L.; Hochella, M. F., Jr. Structure and Bonding Environments at the Calcite Surface as Observed with X-Ray Photoelectron Spectroscopy (XPS) and Low Energy Electron Diffraction (LEED). *Geochim. Cosmochim. Acta* **1991**, *55*, 1723–1736.
40. Stipp, S.; Eggleston, C.; Nielsen, B. Calcite Surface Structure Observed at Microtopographic and Molecular Scales with Atomic Force Microscopy (AFM). *Geochim. Cosmochim. Acta* **1994**, *58*, 3023–3033.
41. Liang, Y.; Lea, A. S.; Baer, D. R.; Engelhard, M. H. Structure of the Cleaved $CaCO_3(10\bar{1}4)$ Surface in an Aqueous Environment. *Surf. Sci.* **1996**, *351*, 172–182.
42. Fenter, P.; Geissbühler, P.; DiMasi, E.; Srajer, G.; Sorensen, L. B.; Sturchio, N. C. Surface Speciation of Calcite Observed *in Situ* by High-Resolution X-Ray Reflectivity. *Geochim. Cosmochim. Acta* **2000**, *64*, 1221–1228.
43. Geissbühler, P.; Fenter, P.; DiMasi, E.; Srajer, G.; Sorensen, L. B.; Sturchio, N. C. Three-Dimensional Structure of the Calcite–Water Interface by Surface X-Ray Scattering. *Surf. Sci.* **2004**, *573*, 191–203.
44. Giessibl, F. J. Atomic Resolution on Si(111)-(7×7) by Noncontact Atomic Force Microscopy with a Force Sensor Based on a Quartz Tuning Fork. *Appl. Phys. Lett.* **2000**, *76*, 1470.
45. Schneiderbauer, M.; Wastl, D.; Giessibl, F. J. qPlus Magnetic Force Microscopy in Frequency-Modulation Mode with Millihertz Resolution. *Beilstein J. Nanotechnol.* **2012**, *3*, 174–178.
46. Pishchik, V.; Lytvynov, L. A.; Dobrovinskaya, E. R. *Sapphire*; Springer US: Boston, MA, 2009.
47. Giessibl, F. J.; Bielefeldt, H.; Hembacher, S.; Mannhart, J. Calculation of the Optimal Imaging Parameters for Frequency Modulation Atomic Force Microscopy. *Appl. Surf. Sci.* **1999**, *140*, 352–357.
48. Israelachvili, J. N.; Pashley, R. M. Molecular Layering of Water at Surfaces and Origin of Repulsive Hydration Forces. *Nature* **1983**, *306*, 249–250.
49. Butt, H.-J.; Cappella, B.; Kappl, M. Force Measurements with the Atomic Force Microscope: Technique, Interpretation and Applications. *Surf. Sci. Rep.* **2005**, *59*, 1–152.
50. Cappella, B.; Dietler, G. Force-Distance Curves by Atomic Force Microscopy. *Surf. Sci. Rep.* **1999**, *34*, 1–104.
51. Kerisit, S.; Parker, S. C. Free Energy of Adsorption of Water and Metal Ions on the [1014] Calcite Surface. *J. Am. Chem. Soc.* **2004**, *126*, 10152–10161.
52. Kerisit, S.; Parker, S. C.; Harding, J. H. Atomistic Simulation of the Dissociative Adsorption of Water on Calcite Surfaces. *J. Phys. Chem. B* **2003**, *107*, 7676–7682.
53. Perry, T. D.; Cygan, R. T.; Mitchell, R. Molecular Models of a Hydrated Calcite Mineral Surface. *Geochim. Cosmochim. Acta* **2007**, *71*, 5876–5887.
54. Imada, H.; Kimura, K.; Onishi, H. Water and 2-Propanol Structured on Calcite (104) Probed by Frequency-Modulation Atomic Force Microscopy. *Langmuir* **2013**, *29*, 10744–10751.
55. Fenter, P.; Kerisit, S.; Raiteri, P.; Gale, J. D. Is the Calcite–Water Interface Understood? Direct Comparisons of Molecular Dynamics Simulations with Specular X-Ray Reflectivity Data. *J. Phys. Chem. C* **2013**, *117*, 5028–5042.
56. Kilpatrick, J. I.; Loh, S.-H.; Jarvis, S. P. Directly Probing the Effects of Ions on Hydration Forces at Interfaces. *J. Am. Chem. Soc.* **2013**, *135*, 2628–2634.
57. Giessibl, F. J.; Reichling, M. Investigating Atomic Details of the CaF_2 (111) Surface with a qPlus Sensor. *Nanotechnology* **2005**, *16*, S118–S124.
58. Watkins, M.; Shluger, A. L. Mechanism of Contrast Formation in Atomic Force Microscopy in Water. *Phys. Rev. Lett.* **2010**, *105*, 196101.
59. Meyer, E.; Güntherodt, H.-J.; Haefke, H.; Gerth, G.; Krohn, M. Atomic Resolution on the AgBr(001) Surface by Atomic Force Microscopy. *Eur. Lett.* **1991**, *15*, 319–323.
60. Meyer, E.; Heinzelmann, H.; Rudin, H.; Güntherodt, H.-J. Atomic Resolution on LiF (001) by Atomic Force Microscopy. *Z. Phys. B* **1990**, *79*, 3–4.
61. Pavese, A.; Catti, M.; Parker, S.; Wall, A. Modelling of the Thermal Dependence of Structural and Elastic Properties of Calcite, $CaCO_3$. *Phys. Chem. Miner.* **1996**, *23*, 89–93.
62. Jacobson, R. L.; Langmuir, D. Dissociation Constants of Calcite and $CaHCO^{3+}$ from 0 to 50°C. *Geochim. Cosmochim. Acta* **1974**, *38*, 301–318.
63. Maslen, E. N.; Streltsov, V. a.; Streltsova, N. R.; Ishizawa, N. Electron Density and Optical Anisotropy in Rhombohedral Carbonates. III. Synchrotron X-Ray Studies of $CaCO_3$, $MgCO_3$, and $MnCO_3$. *Acta Crystallogr. Sect. B Struct. Sci.* **1995**, *51*, 929–939.
64. De Leeuw, N.; Parker, S.; Harding, J. Molecular Dynamics Simulation of Crystal Dissolution from Calcite Steps. *Phys. Rev. B* **1999**, *60*, 13792–13799.
65. Giessibl, F. J. Advances in Atomic Force Microscopy. *Rev. Mod. Phys.* **2003**, *75*, 949–983.
66. Giessibl, F. J.; Bielefeldt, H. Physical Interpretation of Frequency-Modulation Atomic Force Microscopy. *Phys. Rev. B* **2000**, *61*, 9968–9971.
67. Abramowitz, M.; Stegun, I. *Handbook of Mathematical Functions Functions with Formulas, Graphs, and Mathematical Tables*, 9th ed.; Dover: New York, 1972.
68. Raina, G.; Gauldie, R. W.; Sharma, S. K.; Helsley, C. E. A Study of the Calcite Cleavage Plane Using the Atomic Force Microscope. *Ferroelectr., Lett. Sect.* **1994**, *17*, 65–72.